HEFAT2007
5th International Conference on Heat Transfer, Fluid Mechanics and Thermodynamics
1-4 July 2007, Sun City, South Africa
Paper number: CG4

NATURAL CONVECTION FROM MULTIPLE HORIZONTAL CYLINDERS ARRANGED SIDE BY SIDE

C. Cianfrini, M. Corcione* and E. Habib
*Author for correspondence
Dipartimento di Fisica Tecnica, University of Rome "La Sapienza"
via Eudossiana, 18 – 00184 Rome, Italy
e-mail: massimo.corcione@uniroma1.it

ABSTRACT

Steady laminar free convection in air from a row of parallel circular cylinders, is studied numerically. SIMPLE-C algorithm is used for the solution of the mass, momentum, and energy transfer governing equations. Simulations are performed for 10-cylinder assemblies with inter-cylinder spacings from 0.6 to 5 cylinder-diameters and Rayleigh numbers from 10^1 to 10^5. It is found that the thermal performance of the whole assembly increases as the Rayleigh number increases, and has a peak at an optimum separation distance among the cylinders which decreases with increasing the Rayleigh number.

INTRODUCTION

Natural convection heat and momentum transfer from groups of horizontal cylinders set in free space side by side, i.e., arranged in a row, has received not so much attention in the past. In fact, besides a first experimental work conducted by Liebermann and Gebhart [1], who investigated the thermal behavior of an array of ten widely-spaced, long wires at a very low Grashof number, only two other papers on this topic were found in the literature. However, both studies, which were performed numerically by Farouk and Guceri [2], and by Bello-Ochende and Bejan [3], were related to an infinite number of parallel cylinders. Thus, in the absence of data on tube-arrays consisting of a finite number of elements, a short knowledge on both the physical aspects and the actual limits of applicability of the results available for infinite rows of cylinders to real situations, comes out.

In this framework, the aim of the present paper is to investigate free convection in air from a horizontal tube-array consisting of a finite number of horizontal circular cylinders set parallel to one another. The study is conducted numerically under the assumption of isothermal cylinder-surfaces, and two-dimensional steady laminar flow. Simulations are performed for a 10-cylinder assembly with inter-cylinder spacings in the range between 0.6 and 5 cylinder-diameters, and Rayleigh numbers in the range between 10^1 and 10^5. The effects of any independent variable on the flow pattern, the temperature distribution, and the heat transfer rates from any individual cylinder and from the whole assembly, are analyzed and discussed.

PROBLEM STATEMENT

A row consisting of 10 horizontal circular cylinders set parallel to one another, is considered. The diameter D of the cylinders, and the inter-cylinder spacing S, are assigned. Heat is transferred by free convection from each cylinder surface, kept at uniform temperature t_w, to the surrounding undisturbed fluid reservoir, assumed at uniform temperature t_∞.

The buoyancy-induced flow is considered to be steady, two-dimensional, and laminar. The fluid is assumed incompressible, with constant physical properties and negligible viscous dissipation and pressure work. Buoyancy effects on momentum transfer are taken into account through the Boussinesq approximation.

Governing equations

Once the above assumptions are employed in the conservation equations of mass, momentum, and energy, the following set of dimensionless governing equations is obtained:

$$\nabla \cdot \mathbf{V} = 0 \tag{1}$$

$$(\mathbf{V}\cdot\nabla)\mathbf{V} = -\nabla p + \nabla^2 \mathbf{V} - \frac{Ra}{Pr} T \frac{\mathbf{g}}{g} \tag{2}$$

$$(\mathbf{V}\cdot\nabla)T = \frac{1}{Pr}\nabla^2 T \tag{3}$$

where $\mathbf{V}$ is the velocity vector having dimensionless velocity components (U,V) normalized with (ν/D), T is the dimensionless temperature excess over the uniform temperature of the undisturbed fluid reservoir normalized with the temperature difference ($t_w - t_\infty$), p is the dimensionless pressure normalized with ($\rho_\infty \nu^2/D^2$), Ra is the Rayleigh number based on the cylinder-diameter, $\mathbf{g}$ is the gravity vector, and Pr is the Prandtl number.

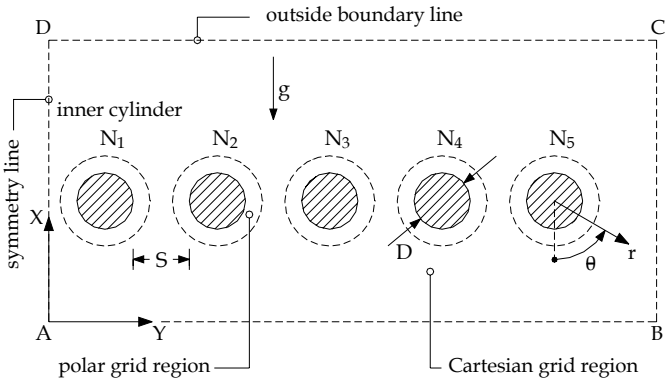

Figure 1 – Geometry, coordinate systems and integration domain

The related boundary conditions are T = 1 and **V** = 0 at any cylinder surface, and T = 0 and **V** = 0 at very large distance from the cylinders.

Computational domain and discretization grid system

The finite-difference solution of equations (1)–(3) with the boundary conditions stated above requires that a discretization grid system is established across the whole two-dimensional integration domain. Since the flow is symmetric about the vertical midplane of the row, the integration domain is taken as a rectangle which includes only one-half of the row, i.e., only five cylinders, and extends from the vertical symmetry midline up to a pseudo-boundary set sufficiently far from the cylinders. A cylindrical polar grid is employed in the proximity of any cylinder, while a Cartesian grid is used to fill the remainder of the integration domain, as sketched in Fig. 1, where the (r, θ) and (X, Y) coordinate systems adopted are also represented. The cylinders are denoted by ordinal numbers N_1 to N_5, where N_1 indicates the inner cylinder, and N_5 the outer cylinder. In the polar systems, U is the radial velocity component, and V is the tangential velocity component. In the Cartesian system, whose origin is taken at the bottom left corner of the integration domain, U is the vertical velocity component, and V is the horizontal velocity component. According to the discretization scheme originally proposed by Launder and Massey [4], the cylindrical polar grids and the Cartesian grid, which are entirely independent of one another, overlap with no attempt of node-matching. Their connection is provided by two sets of false nodes, one for each neighboring grid, located beyond their intersection, as recently described in details by Corcione [5].

Boundary conditions

The boundary conditions required for the numerical solution of the governing equations (1)–(3) have to be specified at any cylinder surface, at the symmetry line and at the boundary lines which enclose the two-dimensional integration domain defined above. In particular, once the pseudo-boundary lines are placed sufficiently far from the cylinders, the motion of the fluid entering or leaving the computational domain may reasonably be assumed to occur normally to them. The entering fluid is assumed at the undisturbed free field temperature. As far as the leaving fluid is concerned, whose temperature is not known a priori, a zero temperature gradient normal to the boundary line is assumed.

The following boundary conditions are then applied:

a) at any cylinder surface

$$U = 0\,, \quad V = 0\,, \quad T = 1 \tag{4}$$

b) at the bottom boundary line A–B

$$\frac{\partial U}{\partial X} = 0\,, \quad V = 0\,, \quad T = 0 \text{ if } U \geq 0 \text{ or } \frac{\partial T}{\partial X} = 0 \text{ if } U < 0 \tag{5}$$

c) at the right boundary line B–C

$$U = 0\,, \quad \frac{\partial V}{\partial Y} = 0\,, \quad T = 0 \text{ if } V < 0 \text{ or } \frac{\partial T}{\partial Y} = 0 \text{ if } V \geq 0 \tag{6}$$

d) at the top boundary line C–D

$$\frac{\partial U}{\partial X} = 0\,, \quad V = 0\,, \quad T = 0 \text{ if } U < 0 \text{ or } \frac{\partial T}{\partial X} = 0 \text{ if } U \geq 0 \tag{7}$$

e) at the left symmetry line A–D

$$\frac{\partial U}{\partial Y} = 0\,, \quad V = 0\,, \quad \frac{\partial T}{\partial Y} = 0 \tag{8}$$

As far as the intersections between polar and Cartesian grids are concerned, the value of each of the dependent variables at any false node of one of the two neighbouring grids is obtained by a linear interpolation of the values of the same variable at the four surrounding real nodes of the other grid.

Solution algorithm

The set of equations (1)–(3) with the b.c.'s (4)–(8) is solved through a control-volume formulation of the finite-difference method. The pressure-velocity coupling is handled by the SIMPLE–C algorithm by Van Doormaal and Raithby [6]. The advection fluxes across the surfaces of the control volumes are evaluated by the QUICK discretization scheme by Leonard [7].

Fine uniform mesh-spacings are used for the discretization of both the polar grid regions and the Cartesian grid region. Starting from assigned first-approximation fields of the dependent variables, the discretized governing equations are solved iteratively through a line-by-line application of the Thomas algorithm, enforcing under-relaxation to ensure convergence. The solution is considered to be converged when the maximum absolute values of both the mass source and the percent changes of the dependent variables at any grid-node from iteration to iteration are smaller than prescribed values, i.e., 10^{-4} and 10^{-6}, respectively.

After convergence is attained, the local and average Nusselt numbers $Nu_i(\theta)$ and Nu_i for the i-th cylinder in the row are calculated:

$$Nu_i(\theta) = \frac{q_i D}{k(t_w - t_\infty)} = -\left.\frac{\partial T}{\partial r}\right|_{r=0.5} \tag{9}$$

$$Nu_i = \frac{Q_i}{\pi k (t_w - t_\infty)} = -\frac{1}{2\pi}\int_0^{2\pi} \left.\frac{\partial T}{\partial r}\right|_{r=0.5} d\theta \tag{10}$$

Table 1 - Comparison of the present results with the benchmark solutions of Saitoh et al.

Ra		$Nu_0(\theta)$ $\theta = 0°$	30°	60°	90°	120°	150°	180°	Nu_0
10^3	Present	3.789	3.755	3.640	3.376	2.841	1.958	1.210	3.023
	Saitoh *et al.* [8]	3.813	3.772	3.640	3.374	2.866	1.975	1.218	3.024
10^4	Present	5.986	5.931	5.756	5.406	4.716	3.293	1.532	4.819
	Saitoh *et al.* [8]	5.995	5.935	5.750	5.410	4.764	3.308	1.534	4.826
10^5	Present	9.694	9.595	9.297	8.749	7.871	5.848	1.989	7.886
	Saitoh *et al.* [8]	9.675	9.577	9.278	8.765	7.946	5.891	1.987	7.898

where q is the heat flux and Q is the heat transfer rate. The temperature gradients at any cylinder surface are evaluated by assuming a second-order temperature profile among each wall-node and the next two fluid-nodes. The integrals are approximated by the trapezoid rule. The average Nusselt number of the whole assembly Nu is then obtained as the arithmetic mean value of the average Nusselt numbers Nu_i of the individual cylinders.

Validation of the numerical procedure

Tests on the dependence of the results obtained on the mesh-spacing of both the polar and the Cartesian discretization grids, as well as on the thickness of the polar grid regions, and on the extent of the whole computational domain, have been performed for several combinations of values of S/D and Ra. In particular, the optimal grid-size values, and the optimal positions of the polar/Cartesian interfaces and the pseudo-boundary lines used for computations (representing a good compromise between solution accuracy and computational time), are such that further grid refinements or boundary displacements do not yield for noticeable modifications neither in the heat transfer rates not in the flow field, that is, the percent changes of $Nu_i(\theta)$ and Nu_i, and the percent changes of the maximum value of the tangential velocity components at θ = 90° and 270° for any cylinder, are smaller than prescribed accuracy values, i.e., 1% and 2%, respectively. Typical features of the integration domain may be summarized as follows: (a) the number of nodal points ($r\times\theta$) of the polar discretization grids lies in the range between 45×72 and 135×90, (b) the thickness of the polar grid regions varies between one-fifth and two times the cylinder-diameter, and (c) the extent of the whole integration flow-domain ranges between 4 and 20 diameters upwards, between 2 and 4 diameters downwards, and between 3 and 8 diameters sidewards, depending on the Rayleigh number and the cylinder-spacing.

As far as the validation of both the numerical code and the meshing procedure is specifically concerned, a comparison between the local and average Nusselt numbers $Nu_0(\theta)$ and Nu_0 obtained for a single cylinder at several Rayleigh numbers and the corresponding benchmark results by Saitoh et al. [8], is reported in Table 1. Moreover, in order to test the reliability of the composite polar/Cartesian grid system at close cylinder-spacing, a comparison between the overall results obtained for a 2-cylinder vertical array and the corresponding experimental data by Tokura et al. [9], are reported in Table 2. Many more details on the code validation are available in reference [5].

RESULTS AND DISCUSSION

Numerical simulations are performed for Pr = 0.71, which corresponds to air, and for different values of (a) the Rayleigh number Ra from 10^1 to 10^5, and (b) the dimensionless inter-cylinder spacing S/D in the range between 0.6 and 5.

Local results are presented in terms of isotherm contours in Figs. 2–4, for Ra = 10^3 and S/D=1, 3, and 5, respectively, and in Figs. 5–7, for S/D=2 and Ra = 10^1, 10^3, and 10^5, respectively.

It may be seen that the mutual interactions occurring among the cylinders give rise to a "suction effect" which causes the rotation of the warm plume spawned by any cylinder towards the center of the row, and, in most cases, their merging. Thus, the lower and upper stagnation points of any cylinder are no longer located at θ = 0° and θ = 180°, respectively, as shown in Fig. 8, where the polar distributions of the local Nusselt number for any cylinder of the right half of the row are reported for Ra = 10^3 and S/D = 1. As for the plume, the more the cylinder is located towards the end of the row, the more the stagnation points rotate with respect to the vertical.

The effects of S/D and Ra on the heat transfer rate from any cylinder are pointed out in Figs. 9 and 10, where the results are expressed through the ratio Nu_i/Nu_0, so as to highlight in what measure the interactions among the cylinders either enhance or degrade the heat transfer performance of the i-th cylinder with respect to that of a single cylinder at same Rayleigh number.

Table 2 - Comparison with the experimental data of Tokura et al.

Nu / Nu_0 for a 2-cylinder vertical array at $Gr = 1.2 \times 10^5$					
	S/D =	1.1	1.3	1.5	2
Bottom cylinder	Present	0.908	0.965	0.996	1.008
	Tokura *et al.* [9]	0.890	0.940	1.000	1.010
Top cylinder	Present	0.614	0.661	0.726	0.853
	Tokura *et al.* [9]	0.610	0.680	0.740	0.870
Whole array	Present	0.761	0.813	0.861	0.930
	Tokura *et al.* [9]	0.750	0.810	0.870	0.940

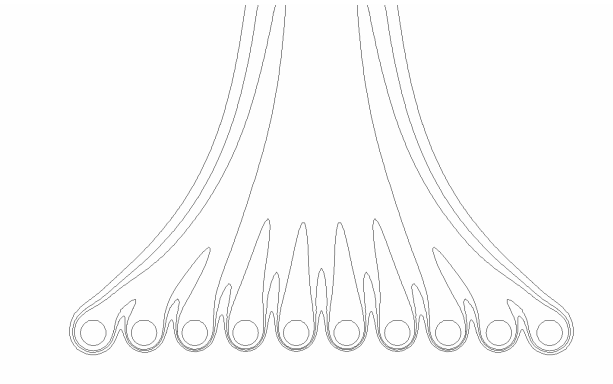

Figure 2 – Isotherm contour plot for Ra = 10^3 and S/D = 1

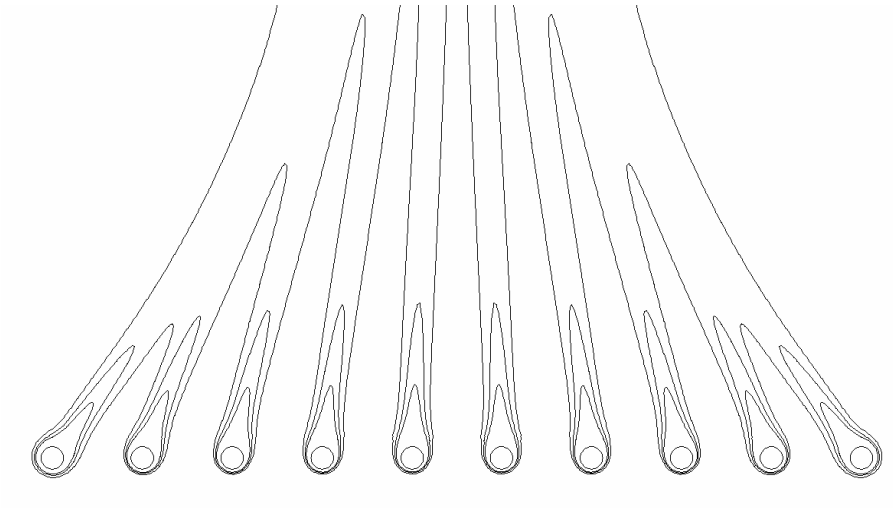

Figure 3 – Isotherm contour plot for Ra = 10^3 and S/D = 3

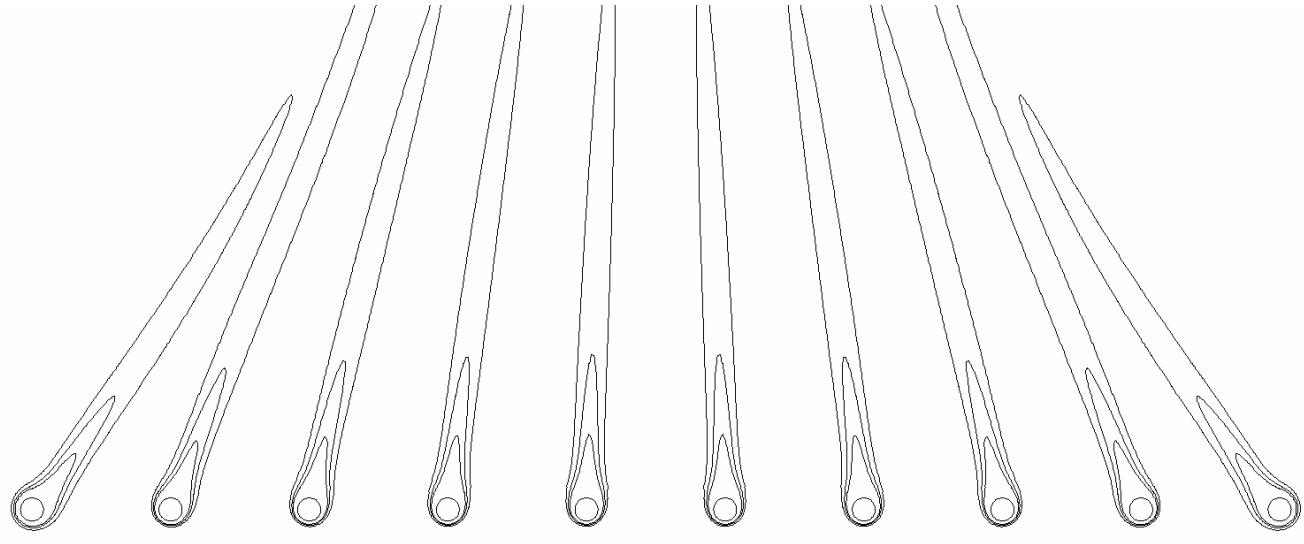

Figure 4 – Isotherm contour plot for Ra = 10^3 and S/D = 5

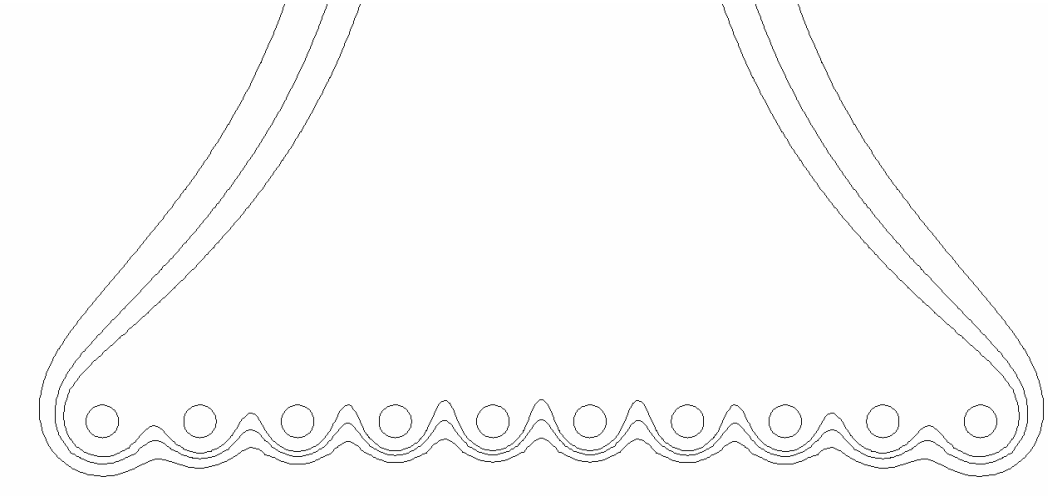

Figure 5 – Isotherm contour plot for Ra = 10^1 and S/D = 2

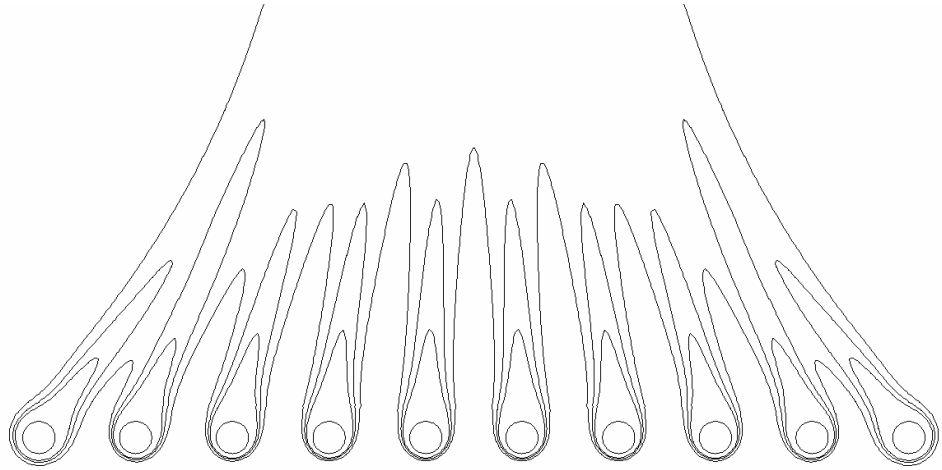

Figure 6 – Isotherm contour plot for Ra = 10^3 and S/D = 2

Figure 7 – Isotherm contour plot for Ra = 10^5 and S/D = 2

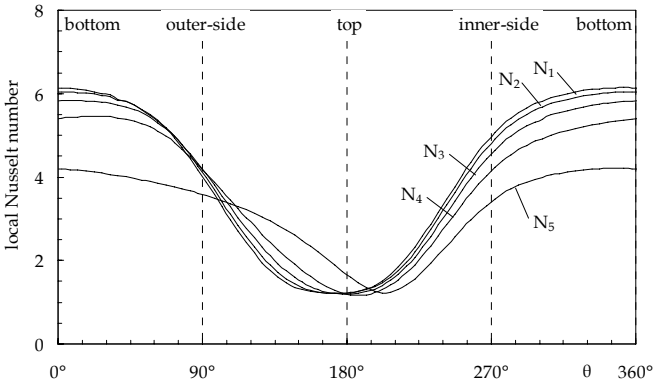

Figure 8 – $Nu_i(\theta)$ vs. θ for $Ra = 10^3$ and $S/D = 1$

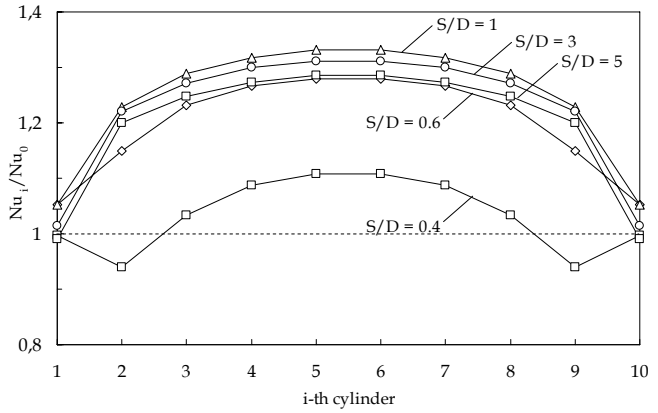

Figure 9 – Nu_i/Nu_0 for $Ra = 10^3$ and different values of S/D

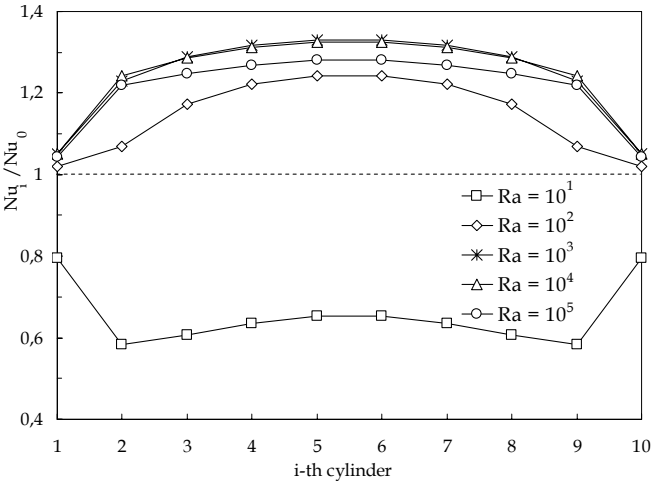

Figure 10 – Nu_i/Nu_0 for $S/D = 1$ and different values of Ra

It is worth noticing that when either Ra or S/D increases, the effects are quite similar, which may be easily pointed out by comparing the distributions of the isotherm lines reported in Figs. 2–4 and in Figs. 5–7. It may be observed that for small values of S/D and/or Ra the behavior of the row resembles that of a horizontal plate, whereas for larger values of S/D and/or Ra the plumes spawned by the cylinders tend to retain their individuality. Also the distributions of Nu_i/Nu_0 vs. N_i evolve following similar paths as S/D and/or Ra increase, as shown in Figs. 9 and 10, where it may be clearly seen that the more the cylinders are located towards the middle of the row, the higher is the amount of heat exchanged at their surface, owing to the suction effect induced by the whole assembly.

What may then be concluded is that both Ra and S/D play roles of the same type. Actually, the temperature field, and thus the amount of heat exchanged at any cylinder surface, depend on how much any cylinder in the row interacts with the neighboring cylinders, which, in its turn, depends substantially on the ratio S/δ between the inter-cylinder spacing and the thickness of the boundary layer. Three different situations may be distinguished: (a) for values of S/δ much larger than unity, the thermal behavior of any cylinder tends to approach that for a single cylinder; (b) for values of S/δ of the order of unity, the interactions occurring between the boundary layers which develop around any cylinder in the row give rise to a kind of chimney-effect with a more or less pronounced increase in the heat transfer rate relative to that for a single cylinder; and (c) for values of S/δ much smaller than unity, the merging of such boundary layers causes a dramatic decrease in the mass flow rate through the cylinders, and then in the amount of heat transferred at their surface. Currently, as the thickness δ of the boundary layer decreases with increasing Ra, it follows that S/δ increases as either S/D or Ra increases, and vice versa. Of course, the thermal behavior of the cylinders located at both ends of the row tends to differ from that of the inner cylinders. In fact, as the outer sides of the end-cylinders which face the free space are not involved in any type of interactions, the heat transfer rate at the end-cylinders is either above or below that for the inner cylinders, according as S/δ is smaller than unity or of the order of unity.

The effects of Ra and S/D on the heat transfer performance of the whole assembly relative to that of a single cylinder Nu/Nu_0, are shown in Figs. 11 and 12.

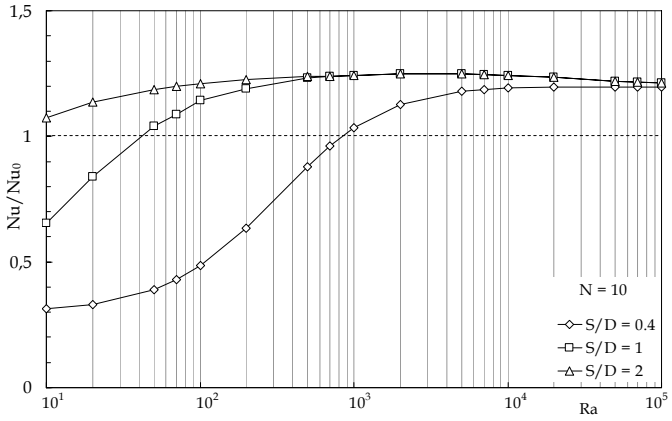

Figure 11 – Nu/Nu_0 vs. Ra for different values of S/D

Figure 11 points out that the value of Ra at which Nu/Nu_0 becomes higher than unity increases as the inter-cylinder spacing decreases. In fact, since the through-flow resistance increases with decreasing S/D, a larger buoyancy force is required to obtain the same heat transfer performance.

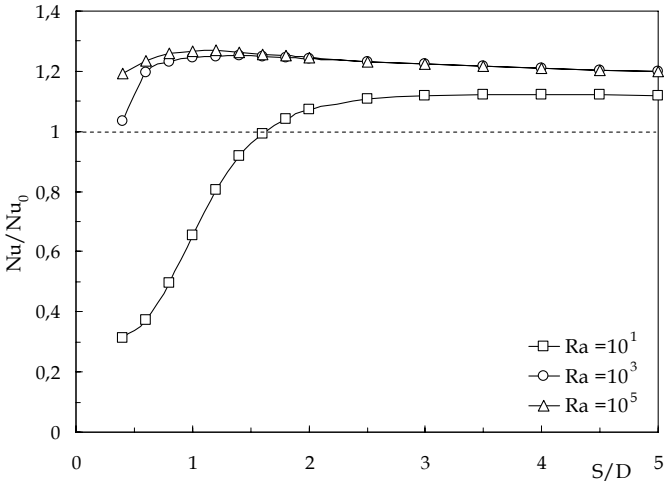

Figure 12 – Nu/Nu_0 vs. S/D for different values of Ra

On the other hand, Figure 12 shows that the positive impact of the convective interactions which occur when the adjacent boundary layers comes in touch is higher at higher values of the Rayleigh number, and that the value of S/D corresponding to the maximum for the average Nusselt number of the whole assembly decreases with increasing the Rayleigh number.

CONCLUSIONS

Free convection in air from a row of 10 circular cylinders, has been studied numerically for inter-cylinder spacings in the range between 0.6 and 5 cylinder-diameters, and Rayleigh numbers from 10^1 to 10^5. It has been found that when the inter-cylinder spacing and/or the Rayleigh number are such that the interactions occurring among the cylinders enhance the heat transfer performance of any cylinder relative to that of a single cylinder, the degree of enhancement for the cylinders located in the middle of the row is higher, due to the suction effect induced by the whole assembly. As far as the overall behavior of the tube-row is concerned, it has been found that the thermal performance of the whole assembly increases as the Rayleigh number increases, and has a peak at an optimum separation distance among the cylinders which decreases with increasing the Rayleigh number.

NOMENCLATURE

D diameter of the cylinders
g gravity vector
g gravitational acceleration
k thermal conductivity of the fluid
Nu average Nusselt number of the row of cylinders
Nu_i average Nusselt number of the i-th cylinder
$Nu_i(\theta)$ local Nusselt number of the i-th cylinder
Nu_0 average Nusselt number of the single cylinder
p dimensionless pressure
Pr Prandtl number = ν/α
Q heat transfer rate
q heat flux
r dimensionless radial coordinate normalized with D
Ra Rayleigh number based on the cylinder diameter = $= g\beta(t_w - t_\infty)D^3/\alpha\nu$
S inter-cylinder spacing
T dimensionless temperature
t temperature
U dimensionless radial or X-wise velocity component
V dimensionless velocity vector
V dimensionless tangential or Y-wise velocity component
X, Y dimensionless Cartesian coordinates normalized with D

Greek symbols

α thermal diffusivity of the fluid
β coefficient of volumetric thermal expansion of the fluid
ν kinematic viscosity of the fluid
θ dimensionless polar coordinate
ρ density of the fluid

Subscripts

i i-th cylinder in the row
w cylinder surface
∞ undisturbed fluid

REFERENCES

[1] J. Lieberman and B. Gebhart, Interaction in natural convection from an array of heated elements, experimental, Int. J. Heat Mass Transfer 12 (1969) 1385-1396.
[2] B. Farouk and S. I. Guceri, Natural convection from horizontal cylinders in interacting flow fields, Int. J. Heat Mass Transfer 26 (1983) 231-243.
[3] T. Bello-Ochende and A.Bejan, Constructal multi-scale cylinders with natural convection, Int. J. Heat Mass Transfer 48 (2005) 4300-4306.
[4] B.E. Launder and T.H. Massey, The numerical prediction of viscous flow and heat transfer in tube banks, J. Heat Transfer 100 (1978) 565-571.
[5] M. Corcione, Correlating equations for free convection heat transfer from horizontal isothermal cylinders set in a vertical array, Int. J. Heat Mass Transfer 48 (2005) 3660-3673.
[6] J. P. Van Doormaal and G. D. Raithby, Enhancements of the simple method for predicting incompressible fluid flows, Numer. Heat Transfer 11 (1984) 147-163.
[7] B. P. Leonard, A stable and accurate convective modelling procedure based on quadratic upstream interpolation, Comp. Meth. in Appl. Mech. Engng. 19 (1979) 59-78.
[8] T. Saitoh, T. Sajiki and K. Maruhara, Benchmark solutions to natural convection heat transfer problem around a horizontal circular cylinder, Int. J. Heat Mass Transfer 36 (1993) 1251-1259.
[9] I. Tokura, H. Saito, K. Kisinami and K. Muramoto, An experimental study of free convection heat transfer from a horizontal cylinder in a vertical array set in free space between parallel walls, J. Heat Transfer 105 (1983) 102-107.